Folding-Unfolding Transitions in Single Titin Molecules Characterized with Laser Tweezers
Author(s): Miklós S. Z. Kellermayer , Steven B. Smith, Henk L. Granzier, Carlos Bustamante
Source: *Science*, New Series, Vol. 276, No. 5315 (May 16, 1997), pp. 1112-1116
Published by: American Association for the Advancement of Science
Stable URL: http://www.jstor.org/stable/2893522
Accessed: 15/10/2010 16:02

Your use of the JSTOR archive indicates your acceptance of JSTOR's Terms and Conditions of Use, available at http://www.jstor.org/page/info/about/policies/terms.jsp. JSTOR's Terms and Conditions of Use provides, in part, that unless you have obtained prior permission, you may not download an entire issue of a journal or multiple copies of articles, and you may use content in the JSTOR archive only for your personal, non-commercial use.

Please contact the publisher regarding any further use of this work. Publisher contact information may be obtained at http://www.jstor.org/action/showPublisher?publisherCode=aaas.

Each copy of any part of a JSTOR transmission must contain the same copyright notice that appears on the screen or printed page of such transmission.

JSTOR is a not-for-profit service that helps scholars, researchers, and students discover, use, and build upon a wide range of content in a trusted digital archive. We use information technology and tools to increase productivity and facilitate new forms of scholarship. For more information about JSTOR, please contact support@jstor.org.

American Association for the Advancement of Science is collaborating with JSTOR to digitize, preserve and extend access to *Science*.

http://www.jstor.org

Soc. London Ser. B **254**, 83 (1993); H. P. Erickson, *Proc. Natl. Acad. Sci. U.S.A.* **91**, 10114 (1994).
11. Titin fragments of interest were amplified by polymerase chain reaction from primary lambda cDNA clones and cloned into pET 9d. NH_2-terminal domain boundaries were as in (*24*). The clones were fused with an NH_2-terminal His^6 tag and a COOH-terminal Cys^2 tag for immobilization on solid surfaces. The identity of the cloned fragments was verified by DNA sequencing with the use of a standard automated sequencer. Expression of the fragments was induced in BL21(DE)3 by 0.1 mM isopropyl-β-D-thiogalactopyranoside at 37°C for 3 hours. The proteins were expressed solubly and were purified from bacterial lysates as described (*25*). Protein was stored frozen in aliquots in 20 mM sodium phosphate (pH 7) and 5 mM dithiothreitol (DTT). Circular dichroism spectroscopy in the far ultraviolet was recorded in storage buffer on a Jasco J-710 spectropolarimeter fitted with a thermostatted cell holder. For further details, see (*1*). The spectra were typical for the beta-barrel structure of titin Ig domains and confirmed the fold of the constructs. Native cardiac titin was purified from bovine heart tissue following the protocol of (*26*), except that the final ammonium sulfate precipitation was omitted. Electrophoresis of the preparation on 3% SDS–polyacrylamide gel electrophoresis showed essentially undegraded titin. The protein was stored at 0.5 mg/ml in 200 mM sodium phosphate (pH 7), 50% glycerol, 5 mM EGTA, 5 mM DTT, and leupeptin (2 μg/ml) at −20°C.
12. The characteristic pattern of the force extension curves observed upon stretching of titin fragments is sensitive to denaturing and cross-linking agents. Incubation of Ig8 in a solution containing 6.6 M urea produced force extension curves that were either featureless or peaked at long extensions with a variable spacing. Treating Ig4 titin fragments with glutaraldehyde (0.1 to 5%) also eliminated the sawtooth pattern in the force extension curves. Instead, we could only observe a featureless and short-ranged force extension curve. These observations suggest that we could either destroy the tertiary structure of the protein by denaturation or that we could render it rigid by cross-linking.
13. It cannot be ruled out that fibronectin III domains, which have a structure similar to that of Ig domains, also contribute to the sawtooth pattern of native titin.
14. The first unfolding peak is typically camouflaged due to multiple adsorptions. The absolute position of the first peak varies because of a random pickup of the protein with respect to the anchoring cysteines, we believe, but also because of rearrangements of the adsorbed segments of the protein on the tip.
15. Note that the unfolding force is the maximum force of the peaks above the baseline of the free cantilever on the approach part of the cycle and not the difference between the peaks and the troughs.
16. Geometric effects can also diminish the observed rupture force of the first peaks. When the line defined by the cysteine tag to the gold surface and the adhesion point on the AFM tip is not in parallel with the direction of pulling, the measured rupture force of the first peak can be up to 15% below the actual force. However, this effect will be unmeasurable from the third peak on.
17. S. Fong *et al.*, *J. Mol. Biol.* **264**, 624 (1996).
18. A. Soteriou, A. Clarke, S. Martin, J. Trinick, *Proc. R. Soc. London Ser. B* **254**, 83 (1993).
19. E. Evans and K. Ritchie, *Biophys. J.* **72**, 1541 (1997).
20. G. I. Bell, *Science* **200**, 618 (1978).
21. H. Grubmüller, B. Heymann, P. Tavan, *ibid.* **271**, 997 (1995).
22. G. Binnig, C. F. Quate, C. Gerber, *Phys. Rev. Lett.* **56**, 930 (1986).
23. G. Binnig and H. Rohrer, *Rev. Mod. Phys.* **59**, 615 (1987).
24. A. S. Politou, M. Gautel, S. Improta, L. Vangelista, A. Pastore, *J. Mol. Biol.* **255**, 604 (1996).
25. A. S. Politou, M. Gautel, C. Joseph, A. Pastore, *FEBS Lett.* **352**, 27 (1994).
26. K.-M. Pan, S. Damodaran, M. L. Greaser, *Biochemistry* **33**, 8255 (1994).
27. C. Bustamante, J. F. Marko, E. D. Siggia, S. Smith, *Science* **265**, 1599 (1994).
28. J. F. Marko and E. D. Siggia, *Macromolecules* **28**, 8759 (1995).
29. Supported by the Deutsche Forschungsgemeinschaft. We thank J. I. Brauman, R. M. Simmons, H. P. Erickson, W. A. Linke, and A. Pastore for helpful discussions and A. Pastore for technical support. J.M.F. was supported by an Alexander V. Humboldt award.

10 March 1997; accepted 9 April 1997

Folding-Unfolding Transitions in Single Titin Molecules Characterized with Laser Tweezers

Miklós S. Z. Kellermayer,*† Steven B. Smith,* Henk L. Granzier,‡ Carlos Bustamante*

Titin, a giant filamentous polypeptide, is believed to play a fundamental role in maintaining sarcomeric structural integrity and developing what is known as passive force in muscle. Measurements of the force required to stretch a single molecule revealed that titin behaves as a highly nonlinear entropic spring. The molecule unfolds in a high-force transition beginning at 20 to 30 piconewtons and refolds in a low-force transition at ~2.5 piconewtons. A fraction of the molecule (5 to 40 percent) remains permanently unfolded, behaving as a wormlike chain with a persistence length (a measure of the chain's bending rigidity) of 20 angstroms. Force hysteresis arises from a difference between the unfolding and refolding kinetics of the molecule relative to the stretch and release rates in the experiments, respectively. Scaling the molecular data up to sarcomeric dimensions reproduced many features of the passive force versus extension curve of muscle fibers.

Passive force develops when a relaxed muscle is stretched; this force is responsible for restoring muscle length after release, and it is required for maintaining the structural integrity of the sarcomere in actively contracting muscle (*1*). Titin (*2*), a giant 3.5-MD protein, spans the half-sarcomere, from the Z line to the M line (*3*) (Fig. 1A). Because titin is anchored both to the Z line and to the thick filaments of the A band, passive force while the sarcomere is stretched is probably generated by extension of the I-band segment of the molecule (*4*, *5*). It has been suggested (*6*, *7*) that the elasticity of titin derives from the reversible unfolding of the linear array of ~300 immunoglobulin C2 (Ig) and fibronectin type III (FNIII) domains (*8*) that make up the molecule. In addition, a unique proline (P)-, glutamate (E)-, valine (V)-, and lysine (K)-rich (PEVK) domain recently identified in titin (*9*) has been hypothesized to form a semistable region that operates as a low-stiffness spring (*9*).

Here, we stretched titin by attaching each of its ends to a different latex bead (*10*), one of which was held by a movable micropipette and the other was trapped in force-measuring laser tweezers (*11*) (Fig. 1B). The micropipette was then moved at a constant rate while the force generated in the molecule was continuously monitored. When a maximum predetermined force (f_{max}) was reached, the process was reversed to obtain the release half-cycle. The force versus extension (f versus z) curves from these experiments (Fig. 2) illustrate several characteristics of the data. (i) The end-to-end distance (z) at which the common f_{max} is reached varies considerably, probably as a result of a variation in the location of the bead attachments in titin. (ii) Many molecules were extended far beyond the ~1-μm contour length of native titin (*12*). (iii) Normalizing the curves to the same length scale reveals that the force generated for a given fractional extension (the ratio of z to the contour length, L) also varies from experiment to experiment, probably reflecting different numbers of titin molecules within the tethers. (iv) All curves show hysteresis.

To identify single-molecule tethers and determine their length, we segregated the data into classes by comparing them with the predictions of two entropic elasticity models: the freely jointed chain [FJC (*13*)] and the wormlike chain [WLC (*14*)] models. The FJC model did not describe the data, but the WLC model fit the stretch data at low to moderate forces and the release data at moderate to high forces (*15*). The WLC model describes the chain as a deformable continuum (rod) of persistence length A, which is a measure of the chain's bending rigidity. For a WLC, z is related to the external force (f) by $fA/k_BT = z/L +$

M. S. Z. Kellermayer and H. L. Granzier, Department of Veterinary Comparative Anatomy, Pharmacology, and Physiology, Washington State University, Pullman, WA 99164–6520, USA.
S. B. Smith and C. Bustamante, Howard Hughes Medical Institute, Institute of Molecular Biology, University of Oregon, Eugene, OR 97403, USA.

*These authors contributed equally to this work.
†Present address: Central Laboratory, University Medical School of Pecs, Hungary.
‡To whom correspondence should be addressed.

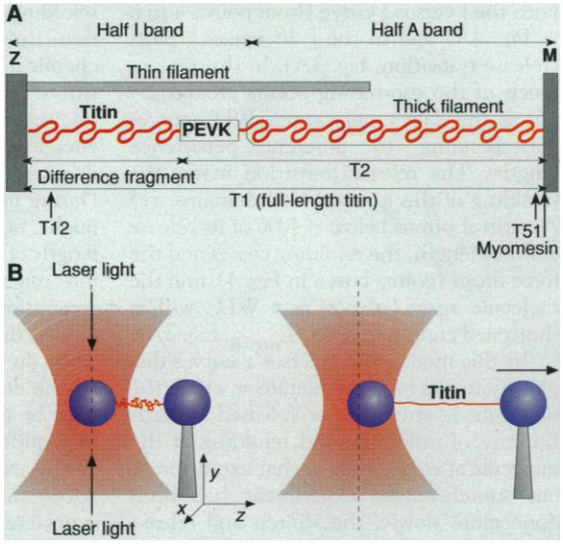

Fig. 1. (**A**) Diagram of the location of titin and the binding sites of the antibodies to titin (T12 and T51) and myomesin in the half-sarcomere. (**B**) Titin molecules were stretched between two beads by moving the micropipette away from the optical trap. The bead in the optical trap (bead at left) was coated with antibody T12, and the other bead was held by a micropipette and bound to the M line end of titin. The end-to-end length (z) was measured as previously described (*11*), and the force on the trapped bead was measured by detecting the change in the light momentum (deflection) as it left the trap (*11*). Use of a coaxial dual-beam optical trap permitted high-force manipulation (~70 pN) far from cover glass surfaces (100 μm) with minimal light power input (100 mW).

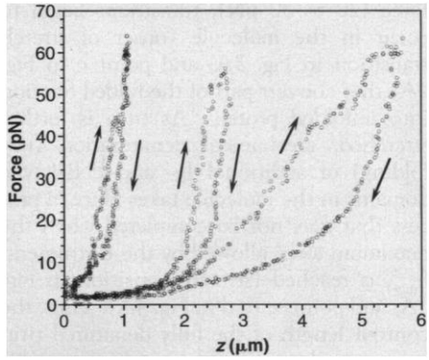

Fig. 2. Ensemble of f versus z curves for three titin tethers. The directions of data acquisition are indicated by arrows. Stretch and release rates were ~90 nm/s.

$1/4(1 - z/L)^2 - 1/4$, where k_B is the Boltzmann constant and T is absolute temperature (*16*). The end-to-end length (z) of a WLC approaches its contour length (L) as $f^{-1/2}$. The contour lengths of the tethers were thus estimated by plotting the data as $f^{-1/2}$ versus z and extrapolating to infinite force (*16*) (Fig. 3A). A histogram of the release contour lengths obtained in this way showed a bimodal distribution with peaks at ~1.5 and ~4 μm (*15*), reflecting the presence of two titin sizes in our preparations [T1 and the difference fragment (Fig. 1A)]. However, there is a discrepancy between the calculated 10-μm contour length for a fully unfolded titin molecule (*17*) and the observed contour-length peak at ~4 μm. Possibly the molecules were never fully unfolded and extended under the forces used (*18*).

In the $f^{-1/2}$ versus z plot, the extrapolated force-axis intercept of a curve at high extension indicates the persistence length of a molecule by the relation $A = k_BT/4F$ [where F is force at the intercept (Fig. 3A)]. When multiple molecules are present in a tether, this intercept (the apparent persistence length of the tether) is divided proportionately. The frequency of apparent persistence lengths for 302 releases of 45 tethers is shown in Fig. 3B. The distribution is multimodal with peaks corresponding to single, double, and triple parallel strands of the molecule. Accordingly, the persistence length of the single, unfolded molecule is ~20 Å. For a given extension, proportionally greater amounts of force were generated when multiple strands of titin were subjected to the stretch-release cycle than when only a single molecule was present (Fig. 3B, inset).

The $f^{-1/2}$ versus z plots revealed that titin does not behave as a WLC throughout the entire stretch-release cycle: Its behavior deviates from that of a WLC at high force during stretch and at low force during release, indicating the onset of structural transitions (Fig. 3A). Because in most experiments the stretch and the release transitions occurred at extensions larger than the contour length of the extended but native titin, these transitions must involve force-induced unfolding and refolding in the molecule. Accordingly, we propose the following model to rationalize these observations: (i) At the beginning of stretch, a variable fraction of the molecule, 5 to 40%, is already unfolded (*19*). In this early part of the stretch curve (WLC region 1 in Fig. 3A, and from points a to c in Fig. 4A), the molecule behaves as a WLC whose properties are dominated by this pre-unfolded fraction. Consistent with this model, $L_{stretch}$ (Fig. 3A) is more than twice as long as the contour length of the native molecule, and the persistence length associated with this part of the curve (20 Å) is about one-seventh that estimated for native titin (*20*). The pre-unfolded fraction may contain the PEVK domain, although in most cases it exceeds the length attributable to this domain (*19*). (ii) As titin is stretched to high

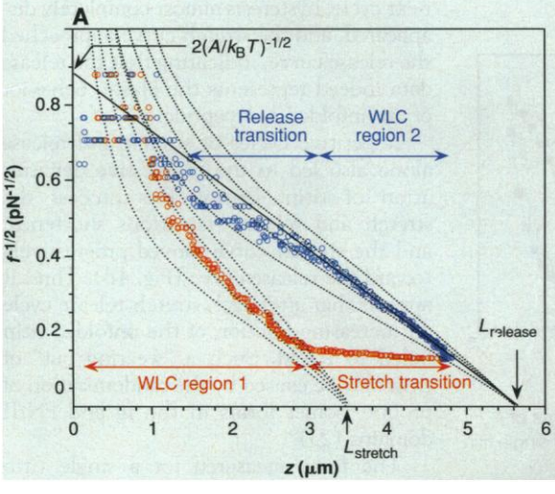

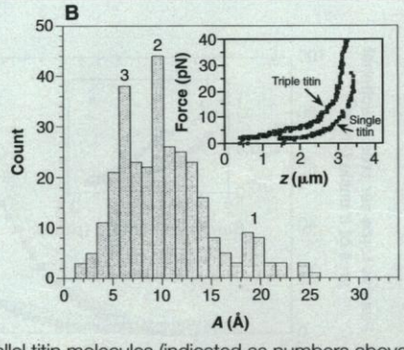

Fig. 3. (**A**) The $f^{-1/2}$ versus z plots for the stretch (red) and release (blue) of a triple-titin tether at a rate of 64 nm/s. A linear fit to the force data at high extension is extrapolated to the z axis to obtain the contour length (L) and to the force to obtain the effective persistence length (A). Dotted lines from left to right are WLC curves for A = 4, 6, 8, and 10 Å for the stretch data, and A = 6, 8, 10, and 12 Å for the release data. (**B**) Histogram of effective persistence lengths showing a multimodal distribution where peaks correspond to various numbers of parallel titin molecules (indicated as numbers above the peaks). The peak at the largest persistence length (~20 Å) was assigned to the single titin molecule. (**Inset**) The f versus z curves (release data) for a triple-titin tether and a single titin molecule. Contour lengths for the two tethers were comparable (4.2 μm for the triple titin and 4 μm for the single).

force (20 to 30 pN), transitions begin to occur in the molecule (onset of stretch transition in Fig. 3A, and point c in Fig. 4A) that convert part of the folded fraction into unfolded protein. As titin is further stretched, mechanical denaturation (unfolding) of additional Ig- and FNIII-type domains in the molecule takes place, a process that may not be completed when the maximum force allowed by the instrument, f_{max}, is reached (stretch transition in Fig. 3A, and points c to d in Fig. 4A). Thus, the contour length of the fully denatured titin was never observed in our experiments. (iii) Upon release of the unfolded titin, the molecule does not refold in the initial ~15 s of the release part of the cycle but behaves instead as a WLC (points d to e in Fig. 4A) with the properties of an unfolded polypeptide (persistence length ~20 Å). (iv) Only when the molecule is allowed to shorten down to about one-half of its release contour length ($L_{release}$) does refolding begin to take place, which is seen as a transition in both the f versus z curve (from points e to b in Fig. 4A) and in the $f^{-1/2}$ versus z plots (release transition, Fig. 3A). In this region, much of the shortening occurs around 2.5 pN as the data cross various WLC curves corresponding to different persistence lengths. The release transition marks the refolding of the Ig and FNIII domains. (v) As titin shortens below ~40% of its release contour length, the refolding ceases and the force drops (points b to a in Fig. 4), and the molecule again behaves as a WLC with a shortened contour length ($L_{stretch}$, Fig. 3A).

In this model, the f versus z curves display hysteresis because the rate at which the molecule is stretched or released exceeds the rate of unfolding and refolding of the molecule at equilibrium at that extension. If our stretch-release experiment had been done more slowly, the stretch and release portions of the force curve would have converged toward a single intermediate curve representing the true equilibrium denaturation-renaturation force. The unfolding and refolding rates under force are much lower than those rates in the presence of strong chemical denaturants (*21*), suggesting that titin's domains must pass through kinetic folding intermediates with high activation energies (E_a), and that pulling a domain does relatively little to lower those energies. During unfolding, such intermediate states might not increase the axial end-to-end length of a domain significantly and therefore might be accessible only through the generation of force perpendicular to the pulling direction (by thermal fluctuations). Thus, an axial force would do little to speed up the denaturation. Tension in the chain must be increased above its folding-unfolding equilibrium value to access these states at the experimental rate. During renaturation under external force, intermediate states are required that would shorten the unfolded domains axially. Tension in the denatured chain will raise the energy of these states, which now stand as barriers (activation states) to renaturation. Therefore, to access these states at the experimental rate, the tension in the chain must be lowered below its equilibrium value. A simulation based on this model reproduces the hysteresis and other features seen in the f versus z curves of Fig. 4 (*22*).

In support of our model, stopping short of the transition in either direction abolished hysteresis. Thus, it was possible to stretch and release the molecule reversibly between points b and c, and also between points d and e in Fig. 4 (Fig. 4A, inset). By comparison, hysteresis was reestablished when either transition was allowed to occur, either in part or to completion. As a further test of this model, titin was stretched in the presence of the chemical denaturant guanidinium-HCl (GuCl) at a concentration of 1.6 M (*6*). Upon addition of GuCl, the molecule exhibited one normal stretch half-cycle but failed to refold on the release half-cycle, so the first stretch-release cycle showed force hysteresis. In the next cycle, hysteresis almost completely disappeared, and the stretch curve approached the release curve, indicating that the release data indeed represents the elastic behavior of an unfolded polypeptide.

Repetitive cycles of stretch and release alone also led to the progressive denaturation of titin. During this process the stretch and release transitions shortened, and the stretch curve moved progressively toward the release curve (Fig. 4B). Thus, it appears that after each stretch-release cycle an increasing fraction of the unfolded titin failed to refold. Such a "wearing out" of titin may be caused by the randomization of proline isomer forms in the Ig and FNIII domains (*23*).

The force measured for a single titin

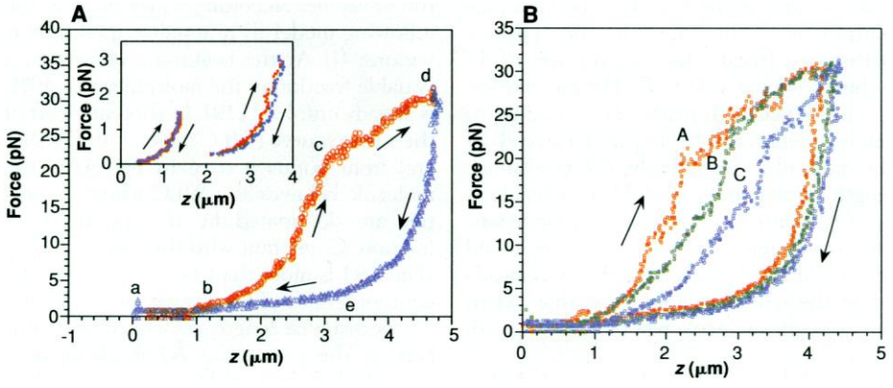

Fig. 4. (A) The f versus extension curve normalized to a single titin molecule (from a double-molecule tether), highlighting the points at the beginning and at the end of the transitions. Both stretch (red) and release (blue) had a rate of ~60 nm/s. **(Inset)** Curves of f versus z for experiments where the stretch or the release of titin was stopped short of entering the stretch or release transition (points c and e, respectively). **(B)** Effect of repetitive cycles of stretch and release in the absence of chemical denaturant. Shown here are the second (A, red), third (B, green), and fifth (C, blue) cycles in a series taken at a rate of 65 nm/s.

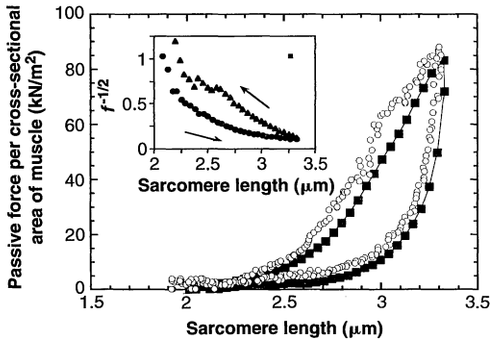

Fig. 5. Calculated passive force per cross-sectional area of skeletal muscle as a function of sarcomere length, scaled up from single-titin data (stretch rate, 65 nm/s, open circles). The scaled-up curve is compared with one obtained for a rabbit m. psoas fiber (estimated stretch rate, 3.3 nm/s, filled squares). Titin density per muscle cross-sectional area was assumed to be $2.8 \times 10^{15}/m^2$ (*4*, *20*). Sarcomere lengths for the scaled-up data were obtained from lengths associated with the fractional extension of the elastic I band segment of titin (*26*), thereby disregarding any difference between the contour length of the I band segment and that of the titin molecules used in the experiments. **(Inset)** Curves of $f^{-1/2}$ versus sarcomere length for the psoas muscle fiber data, showing similar features to those of single titin molecules (Fig. 3A).

molecule can be scaled up by the number of titin molecules in the sarcomere to test the hypothesis that titin is solely responsible for the passive elastic response of muscle. Assuming six titins per thick filament per half-sarcomere (*4*), the calculated curves of passive force per muscle cross-sectional area as a function of sarcomere length can be obtained. The calculated curve is very similar in shape and magnitude to that obtained experimentally for a single skeletal muscle fiber in which caldesmon had been used to block the weak acto-myosin interaction (*24*) (Fig. 5). This agreement validates the previous conclusion (*24*) that titin is the main determinant of the passive force response of muscle. In addition, this analysis indicates that the hysteresis observed in stretch-release experiments in relaxed muscle results from the combined folding-unfolding kinetics of many independent titin molecules (Fig. 5, inset).

It has been argued (*6*, *7*) that domain unfolding-refolding is likely to be involved in the role of titin as an elastic element in muscle physiology. However, if parts of the molecule unfold and refold each time a muscle is stretched and released, an amount of energy equal to the area inside the hysteresis curve would be wasted as heat. We suggest, rather, that the pre-unfolded fraction of titin functions as an efficient (reversible) entropic spring in muscle. Then the purpose of the slow "wearing out" of titin with recent folding-refolding transitions (Fig. 4B) might be to increase the length of the molecule's pre-unfolded region; the longer the pre-unfolded region, the longer also is the range of motion over which the force curve is reversible (regions a to c in Fig. 4A), thereby minimizing subsequent hysteresis and keeping efficiency high. By pre-unfolding just as much titin as necessary, the maximum of the range of efficient elastic response in muscle may be adjusted. Regulating the range of the efficient elastic response in muscle through titin unfolding and refolding may serve as an adaptive mechanism during the repetitive mechanical loading of skeletal or cardiac muscle.

REFERENCES AND NOTES

1. R. Horowits and R. J. Podolsky, *J. Cell Biol.* **105**, 2217 (1987); H. L. M. Granzier, H. A. Akster, H. E. D. J. ter Keurs, *Am. J. Physiol.* **260**, C1060 (1991).
2. K. Wang, *Cell Muscle Motil.* **6**, 315 (1985); K. Maruyama, *Biophys. Chem.* **50**, 73 (1994).
3. D. O. Fürst, M. Osborn, R. Nave, K. Weber, *J. Cell Biol.* **106**, 1563 (1988).
4. H. L. M. Granzier and T. Irving, *Biophys. J.* **68**, 1027 (1995).
5. R. Horowits, E. S. Kempner, M. E. Bisher, R. J. Podolsky, *Nature* **323**, 160 (1986).
6. A. Soteriou, A. Clarke, S. Martin, J. Trinick, *Proc. R. Soc. London Ser. B* **254**, 83 (1993).
7. H. P. Erickson, *Proc. Natl. Acad. Sci. U.S.A.* **91**, 10114 (1994).
8. S. Labeit, M. Gautel, A. Lackey, J. Trinick, *EMBO J.* **11**, 1711 (1992); S. Labeit *et al.*, *Nature* **345**, 273 (1990); J. D. Fritz, J. A. Wolff, M. L. Greaser, *Comp. Biochem. Physiol. B* **105**, 357 (1993); K. M. Pan, S. Damodaran, M. L. Greaser, *Biochemistry* **33**, 8255 (1994).
9. S. Labeit and B. Kolmerer, *Science* **270**, 293 (1995); W. A. Linke *et al.*, *J. Mol. Biol.* **261**, 62 (1996).
10. The Z line end of titin (from rabbit back muscle) was attached to a carboxylated polystyrene bead (3-μm diameter, SpheroTech) coated with protein A to which T12 antibody to titin (*3*) was covalently cross-linked with dimethylpimelimidate (DMP)-HCl (Pierce). The M line end of the molecule was attached either to a polystyrene bead carrying T51 antibody or myomesin [W. J. Obermann *et al.*, *Eur. J. Biochem.* **233**, 110 (1995)], or to an amino-modified silica bead (2.5-μm diameter, Bangs Laboratories) coated with the photoreactive cross-linkers ANB-NOS (*N*-5-azido-2-nitrobenzoyl-oxy-succinimide, Pierce) or sulfo-SANPAH [sulfosuccinimidyl-6-(4′-azido-2′-nitrophenylamino) hexanoate, Pierce]. To tether titin between specific antibodies or myomesin, a microsphere specific for the M line end of titin was captured by a glass micropipette and held by suction. Then a T12-coated bead carrying titin was captured in the optical trap. By tapping the bead on the micropipette against the bead in the trap, connection was established between the two beads through titin, and the molecule was tethered. In the case of a multimolecule tether, the attachment sites of all the involved molecules are likely to be within the small area of bead-to-bead contact, because tapping the beads together was necessary to establish connection. To tether titin by photoreactive cross-linking, a titin-coated T12 bead and a silica bead were tapped together until a temporary linkage was established between them, and this tether was extended to a length of ~2 μm. Finally, ultraviolet (UV) light was projected onto the silica bead by using a quartz optical fiber positioned near the conjugate focal plane of the microscope objective. After titin was tethered, the sample chamber was washed with assay buffer (AB) [25 mM imidazole-HCl, 25 mM KCl, 4 mM $MgCl_2$, 1 mM EGTA, 1 mM dithiothreitol (DTT), pH 7.4] containing 0.2% Tween-20 and T4 lysozyme (0.2 mg/ml) to prevent the nonspecific binding of parts of the titin molecule to any of the beads. Throughout the protocols, AB contained 42 μM leupeptin (Peptides International) and 10 μM E-64 (Sigma). Although the silica beads did not provide sequence-specific attachment, they significantly increased the success of titin tethering.
11. S. B. Smith, Y. Cui, C. Bustamante, *Science* **271**, 795 (1996).
12. K. Wang, M. R. Ramirez, D. Palter, *Proc. Natl. Acad. Sci. U.S.A.* **81**, 3685 (1984); R. Nave, D. O. Fürst, K. Weber, *J. Cell Biol.* **109**, 2177 (1989).
13. W. Kuhn and F. Grün, *Kolloid Z* **101**, 248 (1942).
14. O. Kratky and G. Porod, *Recl. Trav. Chim. Pays-Bas* **68**, 1106 (1949).
15. S. B. Smith, M. S. Z. Kellermayer, C. Bustamante, H. L. Granzier, in preparation.
16. C. J. Bustamante, J. F. Marko, E. D. Siggia, S. B. Smith, *Science* **265**, 1599 (1994); J. F. Marko and E. D. Siggia, *Macromolecules* **28**, 8759 (1995).
17. The length of the fully unfolded, denatured skeletal titin molecule extending from the T12 epitope to the M line is ~10 μm, assuming ~30,000 amino acids (*4*) at 3.5 Å per amino acid.
18. Absence of a uniform distribution of contour lengths out to 10 μm, expected in the case of nonspecific binding by silica beads, could be explained by several mechanisms: (i) the molecules were never stretched beyond half their theoretical length at the forces used; (ii) a fraction of the tethers were loops attached at both ends to one bead and snagged in the middle by the other (this would in turn be a double tether); and (iii) there was specificity in the interaction between titin and silica beads due to the uneven charge distribution along the titin molecule (*25*). The possibility that the transitions in the force versus extension curves could be explained by the presence of multiple molecules of different contour lengths between the beads was excluded by a simulation based on the behavior of WLCs of unequal lengths. This simulation, however, was not used to exclude any multimolecule tether from the data analysis shown in Fig. 3B. Thus, tethers of nonintegral effective persistence lengths in Fig. 3B may reflect such uneven yoking of molecules between the beads.
19. The pre-unfolding contour lengths for various tethers (for example, $L_{stretch}$ in Fig. 3A) varied between 1.5 to 3.0 μm. Assuming this length also included ~1 μm of native titin, the size of the pre-unfolded fraction is 0.5 to 2.0 μm, representing 5 to 20% of the entire ~10-μm-long primary structure. If some of these molecules were tethered in their middles, the pre-unfolded fraction could comprise 10 to 40% of the tethered half-molecule. The unfolded PEVK domain of titin in skeletal muscle, with 2174 residues, may contribute up to 0.8 μm to the contour length of the whole molecule (*4*). Early electron micrographs of titin, which showed the molecule as strings of beads connected with thin strands, have already implied the presence of regions that easily extend or unfold under stress [(*12*); J. Trinick *et al.*, *J. Mol. Biol.* **180**, 331 (1984)]. Recent electron microscopic evidence further points to the presence of an easily unfolding or pre-unfolded region in titin, which may correspond to the PEVK domain (*25*). The relatively small unfolded fraction seen in the electron micrographs could be due to the short time (a few milliseconds per molecule) allowed for denaturation by the preparation procedure.
20. H. Higuchi, Y. Nakauchi, K. Maruyama, S. Fujime, *Biophys. J.* **65**, 1906 (1993).
21. The relaxation time for the force-denaturation of titin was estimated by rapidly stretching the molecule to high force (~60 pN) and holding its length constant while watching the force decay. This relaxation was best fit with a fast decay time of ~4 s and a slower phase of ~70 s. Thus, these processes are slow compared with the stretch and release rates and very slow compared with the ~1 s required to denature reduced-disulfide Ig domains in 4 M GuCl [Y. Goto and K. Hamaguchi, *J. Mol. Biol.* **156**, 911 (1982)].
22. If E_a is increased (or reduced) by the external force (*f*) because the intermediate state is longer (or shorter) than the native (or denatured) state by an amount Δx, the unfolding (or refolding) rate can then be written as $\omega_0 e^{-(E_a - f\Delta x)/k_B T}$, where ω_0 is an attempt frequency set by Brownian dynamics of the peptide chain. The *f* versus *z* curve in Fig. 4 was well fit by assuming E_a = 28 pN·nm and Δx = 0.3 nm for unfolding, E_a = 0 and Δx = 8 nm for refolding, and $\omega_0 = 10^8\ s^{-1}$ for both processes. A refolding intermediate that creates a new fold in the β barrel of an Ig or FNIII domain must shorten the denatured molecule's extension by $\Delta x \approx 8$ nm before the proper set of interactions can be made, but an unfolding intermediate with a high (rate-limiting) free energy could be one in which many bonds or hydrophobic interactions are disrupted by a relatively small shift ($\Delta x \approx 0.3$ nm) away from the ideal shape of the native domain. Source code and simulation results are available at http://alice.uoregon.edu/~cjblab on the Web.
23. The rate of refolding of the FNIII domains could strongly depend on whether or not the unfolding leads to trans-cis isomerization of the eight prolines at the corners of the β folds of these domains [A. L. Main *et al.*, *Cell* **71**, 671 (1992)]. Protein refolding is often limited by the rate of proline isomerization [T. Kiefhaber, H. H. Kohler, F. Schmid, *J. Mol. Biol.* **224**, 217 (1992)]. Because the state of all eight prolines should randomize in a domain that is unfolded for 10 to 100 s, correct isomerization of all eight prolines might take thousands of seconds to occur randomly. Contrary to this view, K. Plaxco *et al.* [*Proc. Natl. Acad. Sci. U.S.A.* **93**, 10703, (1996)] found that an isolated FNIII domain refolded rapidly (<1 s) after chemical denaturation. Titin force-refolding may be slower than FNIII chemical-refolding for several reasons: (i) no residual chemical denaturant helps prevent kinetic traps during refolding, (ii) pulled prolines may preferentially adopt the incorrect cis configuration, (iii) a variety of proline-rich FNIII and Ig domains

are present in titin, and (iv) titin domains are connected axially, limiting their accessible conformations during refolding. Thus, "wearing-out" could still reflect the systematic increase in the number of prolines in the cis state and the consequent increased fraction of slow-to-renature domains in the molecule. Such wearing out may explain why the pre-unfolded fraction of titin was longer than that attributable to the PEVK region. Because all tethers were fully stretched one or more times before data was taken, the pre-unfolded titin could also contain unfolded Ig or FNIII domains that needed more time to renature. Indeed, single molecules recover if left relaxed for several minutes and regain some of their hysteresis behavior. Notably, wearing out and recovery has also been seen in muscle fibers (*24*).

24. H. L. M. Granzier and K. Wang, *Biophys. J.* **65**, 2141 (1993).
25. L. Tskhovrebova and J. Trinick, *J. Mol. Biol.* **265**, 100 (1997).
26. K. Trombitás and G. H. Pollack, *J. Muscle Res. Cell Motil.* **14**, 416 (1993).

27. Supported by grants from the Whitaker Foundation and the National Institute of Arthritis and Musculoskeletal and Skin Disease (AR-42652) to H.L.G., and by grants from NIH (GM-32543) and NSF (MBC 9118482) to C.B. H.L.G. is an Established Investigator of the American Heart Association. The T12 and T51 antibodies were donated by D. O. Fürst. We thank M. Hegner for his help with atomic force microscopy, and G. Flynn, J. Schellman, E. Reisler, G. Yang, K. Campbell, C. Cremo, G. H. Pollack, and B. Slinker for their insightful comments on the manuscript.

10 February 1997; accepted 9 April 1997

Inhibition of Pathogenicity of the Rice Blast Fungus by *Saccharomyces cerevisiae* α-Factor

Janna L. Beckerman, Fred Naider, Daniel J. Ebbole*

Magnaporthe grisea is a fungal pathogen with two mating types, *MAT1-1* and *MAT1-2*, that forms a specialized cell necessary for pathogenesis, the appressorium. *Saccharomyces cerevisiae* α-factor pheromone blocked appressorium formation in a mating type–specific manner and protected plants from infection by *MAT1-2* strains. Experiments with α-factor analogs suggest that the observed activity is due to a specific interaction of α-factor with an *M. grisea* receptor. Culture filtrates of a *MAT1-1* strain contained an activity that inhibited appressorium formation of mating type *MAT1-2* strains. These findings provide evidence that a pheromone response pathway exists in *M. grisea* that can be exploited for plant protection.

The heterothallic ascomycete *Magnaporthe grisea* is a pathogen of a wide variety of grasses but is best known as the causal agent of rice blast disease. The costs of controlling disease with fungicides and the difficulty in breeding durable and effective resistance have led to intense interest in understanding the mechanisms governing the pathogenicity of this fungus (*1*). Conidia of *M. grisea* attach to the plant host with an adhesive that is released from the tip of the conidium upon hydration (*2*). After germination, the fungus responds to contact with the host surface by producing an appressorium, a specialized cell that uses turgor pressure to aid in penetration of the host cell (*3*).

The mating behavior of *M. grisea* is determined by the mating-type locus, which contains either *MAT1-1* or *MAT1-2* DNA. One parent of each of the two mating types participates in a sexual cross. The mating-type loci of filamentous ascomycetes are thought to encode master regulators that control the expression of mating type–specific genes, such as pheromones and pheromone receptors (*4*). In *Saccharomyces cerevisiae*, α-factor and a-factor pheromones are produced by strains with *MAT*α and *MAT***a** mating types. Each pheromone is recognized by a corresponding heterotrimeric GTP-binding protein–coupled receptor expressed in the opposite mating type (*5*).

Appressorium formation of mating type *MAT1-2* strains of *M. grisea* is inhibited when conidia are germinated in the presence of 2% yeast extract. However, 2% peptone and 2% tryptone do not inhibit appressorium formation (*6*). We found that appressorium formation of *MAT1-1* strains was not inhibited by yeast extract to the same degree as *MAT1-2* strains (Table 1). Yeast extract contained an unidentified factor that could be partially purified by an organic extraction procedure designed for purification of small peptides (*7*). This fraction inhibited appressorium formation in *MAT1-2* strains, and the active component appears to be a polypeptide. We found 91 ± 7% appressorium formation of strain 4091-5-8 (*MAT1-2*) with proteinase K–treated extract and 1 ± 1% appressorium formation with untreated extract (*8*). The mating type–specific effect of yeast extract on appressorium formation suggested that *M. grisea* might respond to a pheromone by suppressing infection-related development.

The α-factor pheromone of *S. cerevisiae* has activity in closely related yeast species (*9*). We tested the effect of synthetic *S. cerevisiae* α-factor on *M. grisea* and found that appressorium formation was inhibited in *MAT1-2* strains (Table 1 and Fig. 1, A and B) but not in *MAT1-1* strains (Table 1 and Fig. 1C). The concentration of α-factor needed to cause >95% inhibition of appressorium formation of all *MAT1-2* strains tested was 300 μM. This is 10^4-fold higher than the concentration of α-factor required

Table 1. Mating type–specific inhibition of appressorium formation in *M. grisea*. Conidia were incubated in 50 mM potassium phosphate buffer (pH 6.5) (control), 2% yeast extract, α-factor pheromone in 50 mM potassium phosphate buffer (pH 6.5), or extracts of strain CP987 culture filtrate. Appressorium formation assays were performed as described (*6*). In each of three experiments, a minimum of 300 conidia were counted. The average number of conidia producing at least one appressorium is reported. Variation in appressorium formation between experiments in controls was ±10% or less; appressorium formation in *MAT1-1* strains in yeast extract or CP987 extracts varied by ±20% or less; for *MAT1-1* strains in α-factor, variation was ±10% or less; for *MAT1-2* strains in yeast extract, α-factor, or CP987, extract variation was ±2% or less.

Strain	Mating type	Appressorium formation (%)			
		Control	Yeast extract	α-Factor (300 μM)	CP987 extract
Guy11	1-2	92	0.0	0.8	2.2
4091-5-8	1-2	95	0.0	0.5	0.7
4360-R-12	1-2	92	0.0	0.4	2.2
4375-R-6	1-2	97	0.0	0.0	1.0
CP987	1-1	98	43	91	56
4360-17-1	1-1	96	26	94	44
4136-4-3	1-1	92	50	86	51
4375-R-26	1-1	88	47	91	44
CP2738	1-1	95	45	96	91
CP2735	1-2	93	0.2	0.2	0.2

J. L. Beckerman and D. J. Ebbole, Department of Plant Pathology and Microbiology, Texas A&M University, College Station, TX 77843–2132, USA.
F. Naider, Department of Chemistry, College of Staten Island, City University of New York, 2800 Victory Boulevard, Staten Island, NY 10314, USA.

*To whom correspondence should be addressed. E-mail: dje0282@zeus.tamu.edu